ADVANCED MATERIALS TECHNOLOGIES
www.advmattechnol.de

High Dynamic Range Smart Window Display by Surface Hydrophilization and Inkjet Printing

Qihao Jin, Qiaoshuang Zhang, Junchi Chen, Tim Gehring, Santiago Eizaguirre, Robert Huber, Guillaume Gomard, Uli Lemmer, and Rainer Kling*

Mechanoresponsive smart windows have been intensively investigated in recent years as they offer various applications for signage and light management. However, integrating a display functionality into such smart windows remains a challenge since the realization of pixels in these devices is difficult. In addition, mechanoresponsive smart windows with a high dynamic range are rarely demonstrated because they would suffer from complex fabrication processes and high costs. In this work, a novel surface modification process and digital encoding were developed for direct inkjet printing of micro-etching-masks on hydrophobic elastomers, and a pixelated haze distribution was realized. Compared to the traditional mechanoresponsive smart windows, which modify the optical performance by applied strain solely, here, a smart window with haze tunability in either static or strain-applied state is demonstrated. The work enhances the potential of the fabricated smart window to be applied in high dynamic range signage displays.

1. Introduction

Signage displays, including traffic signs, billboards, and building facade decorations, are omnipresent and essential in daily life. Nowadays, long-lifetime light-emitting diode (LED) displays with high efficiency are widely used. However, the total electrical energy consumption for such displays worldwide is rapidly increasing and contributing to the growing CO_2 emissions.[1,2] Non-emissive displays such as the electronic paper in e-book readers, which contain highly scattering or absorbing microparticles, are much more energy efficient in this regard. Besides, these devices can give high contrast and reflectivity with a near-Lambertian viewing characteristic,[3] which also makes them suitable candidates for signage displays. However, high costs are expected when transferring the electronic paper approach to large-size applications.

On the other hand, smart windows have come to the spotlight in recent years for both interior and exterior applications mainly due to their tunable optical response[4] and low energy consumption.[5] Furthermore, smart windows can be easily integrated into existing infrastructures and buildings, contributing to remarkable energy savings.[6] Inspired by this, turning a smart window into a signage display will be a cost-effective, energy-saving, and environmental-friendly strategy to meet a low carbon footprint. Existing smart windows are commonly based on electrochromism,[7] thermochromism,[8] and switchable liquid-crystal technologies,[9] where the optical transmission and reflection can be manipulated for special purposes, such as privacy protection or sunlight/heat energy management. Among all types of smart windows, mechanoresponsive smart windows are of high interest due to their fabrication simplicity and their potentially low manufacturing costs. Polydimethylsiloxane (PDMS) is a suitable material for such smart windows because of its high optical transmission and stretchability.[10] Moreover, inducing microstructures into PDMS to modulate its optical properties by induced surface wrinkles is a versatile approach.[11,12] It can be easily achieved by the induced strain-difference between the top SiO_x layer and the beneath pristine PDMS, where the former is generated after plasma treatment of the PDMS surface.[13] However, the pixelation on a mechanoresponsive smart window for displaying images in a high dynamic range has not been demonstrated yet. Furthermore, the precise control of the microstructure patterning process for embedding a large number of fine contents, either in the form of images or letters, is yet a considerable challenge. It is because, in the micrometer-scale patterning process, the existing methods are commonly assisted by soft lithography[14] and plasma etching,[15] and are thus highly restrained by imprinting stamps and masks.

Q. Jin, Q. Zhang, J. Chen, T. Gehring, S. Eizaguirre, R. Huber, G. Gomard,[+] U. Lemmer, R. Kling
Light Technology Institute
Karlsruhe Institute of Technology
Engesserstr. 13, 76131 Karlsruhe, Germany
G. Gomard, U. Lemmer
Institute of Microstructure Technology
Karlsruhe Institute of Technology
Hermann-von-Helmholtz-Platz 1
76344 Eggenstein-Leopoldshafen, Germany
E-mail: uli.lemmer@kit.edu

The ORCID identification number(s) for the author(s) of this article can be found under https://doi.org/10.1002/admt.202101026.

[+]Present address: Carl Zeiss AG, Hermann-von-Helmholtz-Platz 6, 76344 Eggenstein-Leopoldshafen, Germany

DOI: 10.1002/admt.202101026

On the contrary, direct inkjet printing of patterned layers or etching masks on the intended surface for surface microstructuring is an economical approach, which brings advantages such as material- and time-saving, flexible design, and fast-prototyping. Inkjet printing, however, can be challenging when the unsuitable surface wettability leads to poor wetting of the printed material and hinders homogeneous and closed thin film formation. The common strategy to convert a hydrophobic PDMS surface into a hydrophilic one is plasma pretreatment. Nevertheless, this is usually a nonstructured process which generates a layer of SiO_x over the entire exposed surface.[16] When this treated PDMS substrate is deformed, the stiff oxidation layer becomes discontinued, and random micro-cracks appear,[17] inducing undesired scattering and deteriorating the optical appearance.[18] This scattering results in an unwanted background haze; therefore, such hydrophilization method is not suitable for PDMS-based mechanoresponsive smart windows that are required to present images with a high dynamic range. In addition, the subsequent printing process will be hindered due to the rough surface.

However, this issue can be tackled by the use of polyvinyl alcohol (PVA), a hydrophilic polymer, which can be dissolved in water and is widely used for adjusting the surface free energy (SFE).[19] So far, direct deposition of continuous PVA thin film on pristine PDMS remains difficult because of wetting issues. The reported PVA deposition methods, including silanization,[20] chemical cross-linking,[21] and pretreatment by plasma,[22] either need hazardous acids or adjust the SFE by eventually forming the unwanted SiO_x layer. Therefore, depositing a homogeneous PVA layer on the PDMS surface in a nondestructive, green, and cost-effective way is yet to be explored. Additionally, the resulted layer is preferred to be ultra-thin and long-term robust. It should also show high surface coverage and exhibit a low surface roughness when applied in optical applications. With such a hydrophilic buffer layer, direct printing of on-surface micro-etching-mask (MEM) with a uniform morphology becomes possible. Besides, it can be further applied in selective microstructure-patterning to tailor the optical properties in smart windows.

In this work, we modified the SFE of PDMS in a solution-based process, leaving the surface intact. Subsequently, a MEM was inkjet printed on PDMS, allowing for a laterally defined patterning of microgrooves by plasma treatment. This enables to locally modify the light scattering in a mechanoresponsive smart window. With our novel thermal-enhanced surface modification process, the size of the MEM and subsequent microgroove patterns allow a minimal feature size down to the 10 μm length scale. Compared to the traditional mechanoresponsive smart windows, we managed to modify the haze not only in the strain-applied state, but also in its static state. The latter was realized by carefully defining the light scattering in a pixelated manner. The haze level in the smart window can be therefore controlled locally, continuously, and linearly via the MEM design. Accordingly, high image sharpness and a 225 available haze depth at each unit area were realized. Our approach managed to demonstrate a mechanoresponsive smart window that can present images with a high dynamic range, which can be utilized in signage display applications.

2. Results and Discussion

To deposit an ultra-thin PVA layer on pristine PDMS, a novel thermal-enhanced surface modification process was developed. We first investigated the deposited PVA thin-film quality for various solution temperatures. PDMS films were immersed in PVA solutions with different temperatures, that is, room temperature (≈23 °C), 40, 60, 80, and 100 °C, for 1 h. The films remained in the solution until the whole solution cooled down to room temperature. Afterward, the samples were dried in nitrogen flow, and static water contact angle (SWCA) measurement was performed on each surface. The results are shown in **Figure 1**a. It can be seen that, compared to the SWCA (113°) on pristine PDMS surface, as shown in Figure 1b, all the surfaces after PVA solution immersion show a decreased SWCA, indicating an increased SFE caused by the PVA deposition. When the PVA solution temperature was between 23 and 80 °C, the measured SWCAs are all around 70°. However, when the temperature was increased to 100 °C, the SWCA decreases to 60° as shown in Figure 1c. For each temperature, 40 SWCA measurements were carried out. Accordingly, the standard deviation of the SWCA, shown as the error bar in Figure 1a, can be interpreted as an indicator of the PVA-deposition homogeneity. It shows a clear tendency that the standard deviation declines with the temperature, implying an increased homogeneity of the deposited PVA layer. For either SWCA or PVA-deposition homogeneity, the treating condition with 100 °C temperature outperforms the others. To characterize the surface roughness of the modified surface, atomic force microscopy was applied. It shows only a slight increase in the peak-to-valley roughness when comparing the pristine (Figure 1d) with the modified surface (Figure 1e). The few small grains on the latter likely resulted from the crystallization of PVA during adsorption.[23] The corresponding root mean square (RMS) roughness on the treated surface was around 1.4 nm, indicating a fairly smooth layer. Besides the surface homogeneity and roughness, the thickness of the deposited layer is important, because a thick PVA layer can cause unwanted optical scattering when applied in a device that requires precise optical behavior control.[24] To measure the thickness of the PVA layer deposited with 100 °C, an optical profilometer was used. The value was about 10 nm (see Figure S1, Supporting Information). Due to its ultra-low thickness, no distinguishable differences in total optical transmittance and haze were observed in the spectra between 380 and 780 nm compared to the pristine PDMS (see Figure S2, Supporting Information). Here, haze is used to describe light scattering by the resulting layers quantitatively and is defined as the ratio of the diffuse fraction of the transmitted light to the overall transmitted light.

The improved surface property after PVA modification becomes evident in the subsequent MEM printing process. We used poly(methyl methacrylate) (PMMA) as the material of the MEM, and compared the PMMA surface coverage by inkjet printing it on differently treated PDMS with a droplet spacing of 21 μm. Figure 1f shows the microscope image of the printed PMMA layer on the pristine surface. It can be seen that the inkjet-printed PMMA shrunk to isolated islands due to the poor surface wettability on the pristine PDMS. Then we compared the printed PMMA on PVA-solution-treated

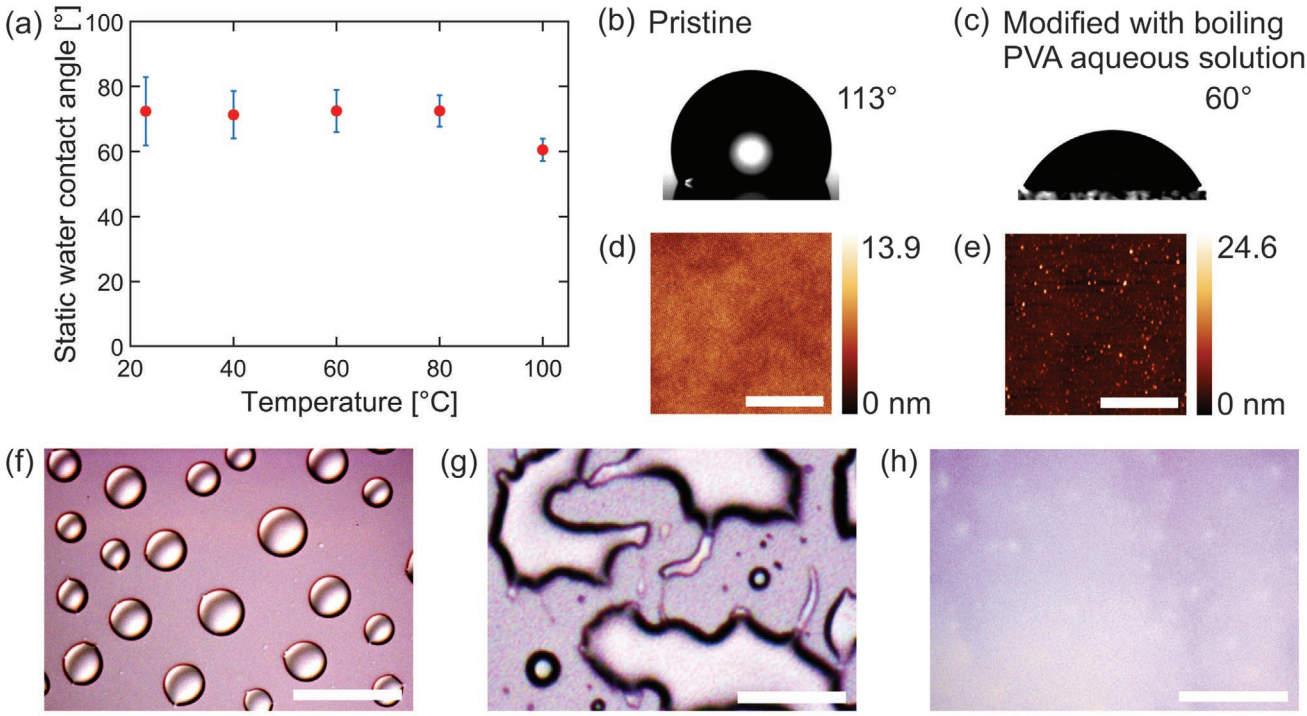

Figure 1. a) Static water contact angles on the PDMS surfaces treated with solution temperatures of ≈23, 40, 60, 80, and 100 °C, respectively. The error bar represents the standard deviation. b,c) Static water contact angles on pristine and 100 °C-solution-treated PDMS surfaces, respectively. d,e) AFM images of pristine and 100 °C-solution-treated PDMS surfaces, respectively. Scale bar: 1 µm. f) Optical images of inkjet-printed PMMA layer on pristine PDMS surface. Scale bar: 100 µm. g,h) Optical images of inkjet-printed PMMA on PDMS surfaces treated with solutions of ≈23 and 100 °C, respectively. Scale bar: 100 µm.

PDMS surfaces but with different treating temperatures. The optical images of the formed PMMA layer are presented in Figure 1g,h, where the PDMS surface in Figure 1g was treated with PVA at room temperature, and the one in the Figure 1h was treated with PVA at 100 °C. As can be seen, the PMMA on room-temperature-treated PDMS surface was discontinuous while a closed PMMA film was formed on the surface treated with 100 °C solution. The poor film formation quality shown in Figure 1g indicates that the PVA surface coverage and quality under room-temperature treatment was not sufficient compared to that obtained after the boiling treatment. We note that the inkjet printed PMMA shows much stronger effects than the mere 10° in the SWCA measurement. We attribute this difference to the much smaller droplet size in the inkjet printing process compared to the SWCA measurement. Therefore, the PMMA wetting behavior is much more sensitive to the homogeneity of the PVA layer. The mechanism behind the thermal-enhanced PVA coverage might be explained by the combined effect of the natural crystallization of PVA molecules,[25] and the boiling-water-generated surface hydroxyl group from residual -SiH functional groups in PDMS, which enhances the bonding between PVA and PDMS.[26]

Moreover, a lifetime investigation of the modified surface was performed by the SWCA measurement, which is used to verify the robustness of the PVA layer. As shown in Figure S3a, Supporting Information, after storing the modified PDMS in the air for 100 days, the SWCA remained almost the same as before (60°). Additionally, Figure S3b, Supporting Information shows that, after being immersed in ambient water for the same period, the SWCA on the modified surface was increased only by 6.5°. Based on these results, it can be deduced that our method of water-based thermal treatment is a straightforward, durable, nondestructive, and cost-effective method for PDMS surface hydrophilization. In addition, the bio-compatibility and longtime stability of both the PVA and the subsequently modified PDMS offer more potential for versatile applications such as bio- and sensing technologies.[24,27] Another advancement of our developed surface modification is the elimination of a pretreatment before PVA deposition. Moreover, our approach does not require additional chemicals for intermediate molecules linking. Besides, after the direct PVA surface deposition, the high optical transmission and the low surface roughness of the PDMS beneath are preserved to the largest extent.

With the developed method, it becomes possible to print a PMMA-based MEM on PDMS with variable 2D designs, ranging from dots and lines to homogeneous thin films in a highly controllable manner. The printed MEM can then be used to pattern a surface with proper plasma treatment, inducing pixelated images or information into a smart window. Before the actual smart window patterning process, we investigated the haze level over the different initial stretching ratio of PDMS treated in plasma. The purpose is to find the best ratio for inducing a haze that is high and steady over the entire visible wavelength range. Accordingly, four stretching ratios were applied for the comparison, which were 1.2, 1.4, 1.6, and 1.8. The ratio was calculated as the length in stretching over the

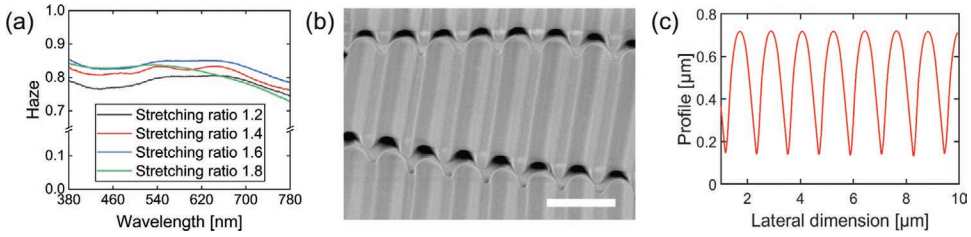

Figure 2. a) Haze comparison of fabricated PDMS films with different stretching ratio applied during plasma treatment. b) SEM image of microgrooves generated by plasma treatment after releasing the PDMS film. The film was stretched with a ratio of 1.6. Scale bar: 2 μm. c) Profile of the microgrooves in (b) (taken from the highlighted path in Figure S4, Supporting Information).

initial length. **Figure 2**a shows the results of spectral haze comparison. It can be found that the PDMS with a stretching ratio of 1.6 shows the desired performance. Figure 2b is the scanning electron microscopy (SEM) image of the generated microgrooves on the released film, and Figure 2c shows the profile of the wrinkled structure measured from the highlighted line in Figure S4, Supporting Information. As can be seen, the microgrooves are highly ordered and continuous in the lateral direction but are separated along the direction of the microgrooves into individual segments. These segments result in numerous edges and increase the optical light scattering by the edge effect,[28,29] which contributes to the optical haze in the released film. Therefore, by designing proper MEMs, pixelated patterns can be embedded into smart windows to display information. Moreover, based on the light scattering from the edge effect, manipulating the haze level via controlling the induced edge density on a smart window becomes possible.

To illustrate the strategy of realizing a pixelated smart window, **Figure 3**a–c show the schematic of the fabricating procedure in our work. First, the surface of a prestretched (stretching ratio 1.6) PDMS film was modified by the developed thermal-enhanced process, as seen in Figure 3a. Second, in Figure 3b, the MEM was inkjet printed on the modified surface, intending to cover the area selectively. The MEM in this figure is depicted as a gradient ink coverage (IC) to enable a lateral tunable haze in a static smart window. Then the film was treated in oxygen plasma, as shown in Figure 3c, where only the top surface printed with MEM was exposed to the plasma while the bottom side was attached with a piece of glass. The glass can protect the bottom surface from plasma treatment, and this avoids the unwanted microstructure being formed. In the end, the PDMS film was immersed in acetic acid for 5 min to remove the MEM residuum (PMMA) and released from the stretched state. To this point, the periodic microgrooves were induced only on the exposed surface, forming a pattern that was defined by the printed MEM. Figure 3d shows schematically that the fabricated smart window can present a linearly tunable haze in the lateral direction. This haze tunability does not require stretching and is realized by pixelated light scattering. Furthermore, the induced pattern can be switched between visible and invisible states upon stretching (Figure 3e). Compared to the traditional mechanoresponsive smart windows, our approach allows to achieve patterns which are not only able to response to the applied strain, but also pixelated for increased haze depth. This further leads to higher information amount in the smart window.

Subsequently, we demonstrate the quantization of the induced haze depth with the approach mentioned above. In order to induce controllable edge density and generate different haze levels locally in a pixelated smart window, 8-bit gray-scale

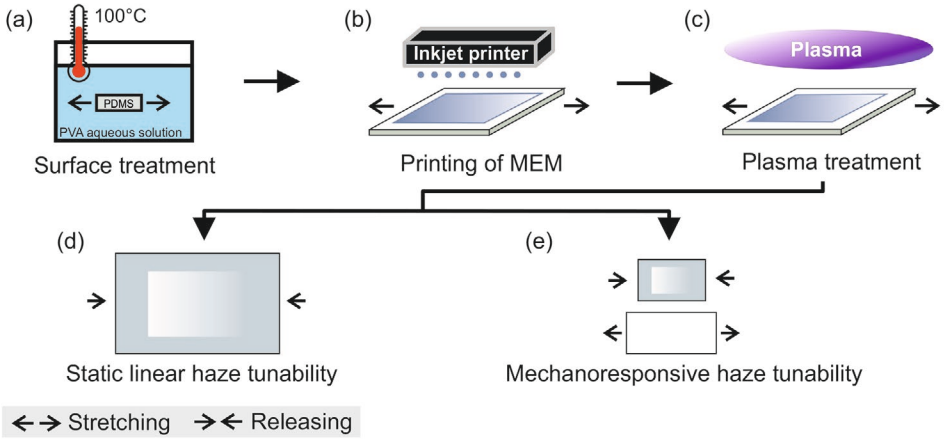

Figure 3. Schematic illustration of the procedure to prepare the smart windows. a) Surface treatment of a stretched PDMS film in 100 °C PVA solution. b) Inkjet printing of MEM onto the modified and stretched PDMS film. The MEM is printed with gradient ink coverage in the lateral direction. The glass on the bottom side of the PDMS film is not shown. c) Plasma treatment of the MEM-printed PDMS film. d) Schematic illustration of linear haze tunability in a smart window without stretching. e) Schematic illustration of the mechanoresponsive haze tunability in a smart window upon stretching. For both (d) and (e), the microgrooves are induced in the area without MEM and presented as a gray color. The area presented as white color is transparent and without haze.

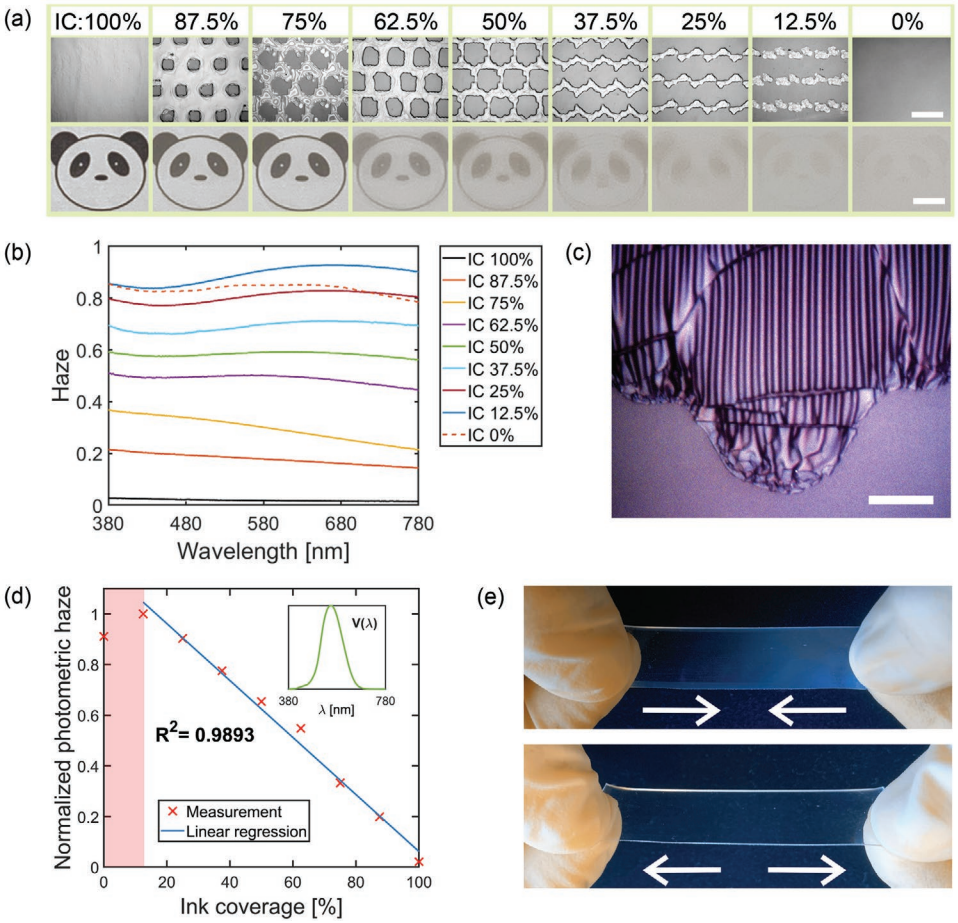

Figure 4. a) The first row shows the optical images of different inkjet-printed MEMs on PDMS. Each MEM pattern corresponds to the respective ink coverage (IC) shown above the respective image. Scale bar: 200 µm. The second row shows the haze-induced PDMS films (stretching ratio: 1.6, treated by plasma with the respective MEM above) on top of a black and white panda cartoon. All the PDMS films were in the released state. Scale bar: 4 mm. b) Spectral-dependent haze level of each PDMS film presented in (a). The haze was induced by the MEM with different ICs. The dashed line is the spectral haze curve that belongs to IC of 0%. c) Optical image of microgrooves-consisted pattern with a zoomed-in view. The microgrooves close to the boundary are irregular. Scale bar: 15 µm. d) Linear regression of photometric haze over GS values. The coefficient of determination R^2 is 0.9893. The insert is the photopic luminous efficiency function $V(\lambda)$. The red marked zone between IC of 0% and 12.5% is excluded during mask design. e) Optical images of a PDMS film that exhibits 2D haze tunability, that is, gradient haze tunability in static state, and two-state (translucent and transparent) switchability upon stretching.

(GS) mask patterns were designed and then converted to 2-bit (black/white) printing recipes by halftone reprography. The correlation of the GS and designed MEM pattern can be seen in Figure S5, Supporting Information, where the black color represents the ink-covered area. Although the GS value during the MEM design can be directly used for the final haze level control, we here use IC as a more straightforward indicator to illustrate the developed process of haze manipulation. The corresponding ICs of GS values are listed in Table S1, Supporting Information. To obtain intended IC on individual surfaces, different MEMs were designed. **Figure 4**a shows an overview of the printed MEMs used to achieve different haze levels in the PDMS films. The first row therein shows microscope images of the printed MEMs with different IC as indicated above the respective image. The very left image shows the area fully covered with PMMA (IC = 100%), and the very right one is the area without a mask (IC = 0). After plasma treatment and MEM residuum removal, the microgrooves and thus haze are induced onto the film in the unmasked areas after the film was released. The second row in Figure 4a shows images of films with different haze placed on top of a black and white panda cartoon. Each film was treated by plasma with the respective MEM shown in the row above. As can be seen therein, with the increased haze levels of the films from left to right, the underneath panda image becomes gradually blurred. It has to be noted that all the films above the panda cartoon were in the released state, and the individual haze level of the films was achieved by the MEM design only, that is, without applying mechanical stretching.

To define the haze level quantitatively, the spectral dependency of haze in each released film was measured, and the results are plotted in Figure 4b over the visible light range. The haze levels are steadily increasing with decreasing IC. For lower ICs, the haze levels are approaching 1, that is, no direct transmission. However, a decrease in the haze is observed for the IC of 0 (the dashed line in the figure) compared to the IC of 12.5%. The reason could be that, while the IC is approaching

0, more surface areas were exposed to plasma and turned into microgrooves. Thus, the contribution of optical scattering, which resulted from the boundary between the structured and pristine surface, became less prominent. This notion is supported by Figure 4c, which is the optical image of the generated microgrooves pattern from a MEM with an IC of 50%. At the edge of the pattern, the irregular microgrooves induce more light scattering compared to the other regions.[28,30–32] Furthermore, in order to take the spectral sensitivity of the human perception into consideration, for each IC, the corresponding haze spectra were weighted by the standard photopic luminous efficiency function $V(\lambda)$[33] and were integrated over the visible light range. This yields one single value, which we define as photometric haze here. The values resulted from the different IC are plotted in Figure 4d. A linear dependence is observed in the IC range from 12.5% to 100%, and the monotonicity breaks at IC = 0. To achieve a linear haze controllability in our smart window, all the MEMs were designed with IC located in the linear region, while the IC region below 12.5%, which is marked as red zone in Figure 4d, was excluded. It is found that the corresponding linear regression (from IC = 12.5% to 100%) has a coefficient of determination R^2 of 0.9893, implying a good quantitative control of the photometric haze by linearly tuning the IC. Since the IC is initially determined by the GS during the digital MEM design, a 225 haze depth can be achieved accordingly (GS from 0 to 224, step of 1). To demonstrate this high haze depth and linear haze tunability in a smart window, a MEM designed with gradient IC (from 100% to 12.5%) was printed on PDMS. The released film after plasma treatment is shown in the upper part of Figure 4e, where the haze level increased gradually from the left (fully transparent) to the right (high haze level) side. Furthermore, the entire smart window can be made transparent upon stretching, as shown in the lower part of the same figure. This 2D haze modulation, referring to site-to-site and mechanoresponsive haze tunability, can therefore be applied in smart window signage displays to deliver information with a high dynamic range.

To utilize this well-controlled haze modulation in a smart window display, a patterned PDMS film was subsequently fabricated. **Figure 5**a presents a photo of roses, which was then converted to a GS image by halftone reprography, as shown in Figure 5b. The MEM was then printed following this pattern to introduce the image into the PDMS film. Figure 5c shows the optical image of the fabricated smart window (film in the released state) with a black color background. It can be seen that the pattern in the smart window display was replicated from the rose photo. In addition, it is worth mentioning here that the brightest spot in the GS image design was defined as GS = 224 while the black was defined as GS = 0; that is to say, the haze levels in the smart window display were controlled in the linear zone by the digital encoding. Figure 5d,e show the mechanoresponse in our smart window display, where the image stored in it can be switched between transparent (stretched) and visible (released) states, respectively. To further demonstrate that the presented image can be observed even at a large viewing angle as in the electronic paper, an optical image was taken from the side of the rose pattern (≈60° to the surface normal) under sunlight illumination, as seen in Figure 5f. It shows the reflective scattering view of the smart window display. As can be seen, the rose pattern is clearly presented, preserving the original image quality to a large extent. This good performance indicates the potential of our smart window to be applied in the display applications that require a high dynamic range.

3. Conclusion

In conclusion, we have presented a versatile approach for realizing a smart window with the possibility to integrate a signage function. A water-based and thermal-enhanced process

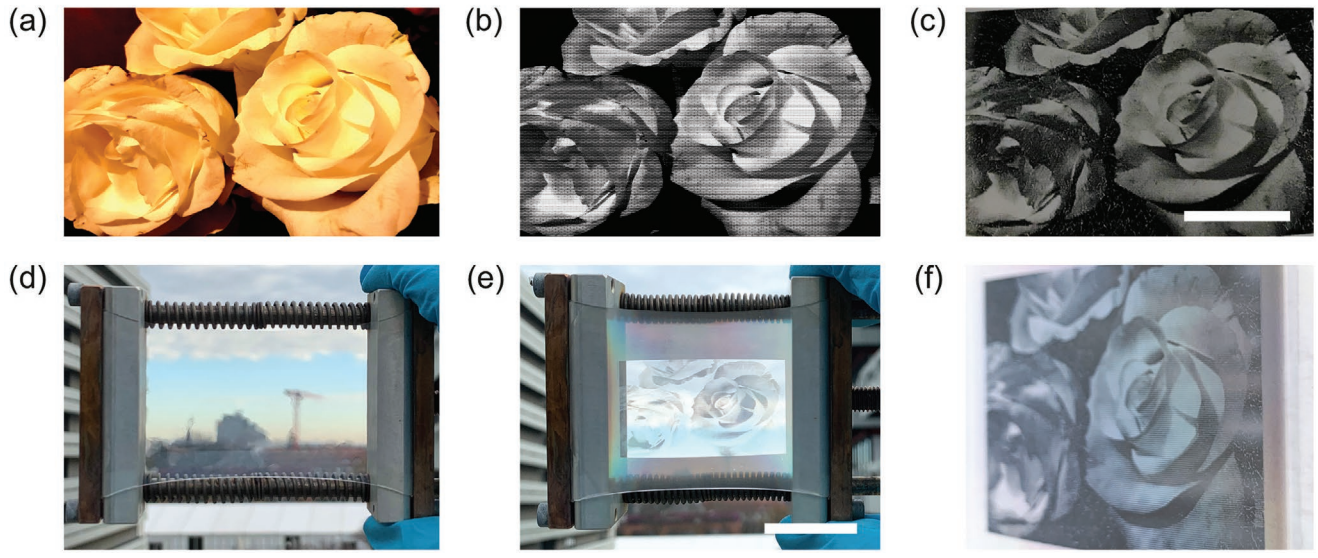

Figure 5. a) Optical image of rose flowers used for smart window display design. b) Converted GS image from the image in (a). c) Optical image of the released smart window. Scale bar 10 mm. d) Optical image of the view through the smart window upon stretching in the transparent state. e) Optical image of the smart window in the released state showing the rose pattern. Scale bar 20 mm. f) Optical image of the reflective scattering view of the released smart window observed at a large viewing angle (≈60° to the surface normal).

was developed for PDMS surface modification using a boiling process in an aqueous PVA solution, enabling a controlled deposition of PMMA layers on the modified PDMS films by inkjet printing. PMMA-based MEM with spatial pattern was designed with digital encoding and was directly inkjet printed on the modified PDMS in a remarkably flexible and precise manner. Hereby, we achieve a highly controllable microgroove patterning and a spatially controlled light scattering based on the edge effect. A continuous and linear tunability of the photometric haze was successfully demonstrated using this method. Depending on these, an energy-saving smart window display with a high dynamic range was fabricated with a 225 available haze depth.

4. Experimental Section

Fabrication of PDMS Slice: PDMS slices were prepared by first mixing the silicone elastomer with a curing agent (Sylgard 184, Dow) at a weight ratio of 10:1. And then, the mixture was degassed in a vacuum desiccator for 30 min to remove air bubbles. Afterward, a certain volume of the precursor was dropped on a glass substrate by a syringe. The glass was placed on a hot plate with a minimized vertical tilt under room temperature. After the precursor covered the entire glass surface by self-leveling, the temperature of the hot plate was first increased to 50 °C for 10 min, and then increased to 95 °C for 10 min. The PDMS slice was subsequently peeled off the glass, and the thickness was around 1 mm.

PVA Surface Modification: The PVA aqueous solution was prepared by first adding PVA (98–99% hydrolyzed, high molecular weight, Alfa Aesar) in distilled water at 100 °C with a concentration of 0.2 wt%. Then the solution was stirred for 15 min. The temperature of the solution was subsequently reduced to 95 °C, and the solution was continuously stirred for 1 h. For the surface treatment of PDMS with PVA solution, PVA solutions were prepared at five different temperatures to investigate the gradient temperature effect, that is, room temperature (≈23 °C), 40, 60, 80, and 100 °C. Each stretched PDMS slice was immersed in the respective solution for 1 h. During treatment, a certain amount of distilled water was added to maintain the original weight of the solution. After the solution was naturally cooled down to room temperature, the PDMS slices were dried with nitrogen flow and were kept in the stretched status for inkjet printing.

Inkjet-Printing of MEMs: PMMA with a molecular weight of 65 000 Da (PSS-polymer) was used as the material of MEM. The PMMA was first dissolved in 1,3-dimethoxybenzene (≥98% Sigma-Aldrich), and then 10 vol% hexylbenzene (97% Sigma-Aldrich) was added to the solution. In the end, a final concentration of 80 mg mL^{-1} was achieved. One nozzle was used for printing with an inkjet printer (Pixdro LP50), and a 1 pL cartridge (Fujifilm Dimatix) was used. The print head temperature was set to 32 °C, and a custom-made waveform with a maximum voltage of 19 V was applied to achieve an optimized performance for up to 2.5 kHz jetting frequency. The digital patterns of the MEMs with a resolution of 1200 dpi were generated by halftone reprography and were applied subsequently as the printing recipes. After printing, the printed MEMs were dried at room temperature in ambient conditions.

Surface Microgrooves Generation: The stretched PDMS was treated by oxygen plasma in a UVO plasma cleaner (Femto, Diener electronic) under a pressure of 40 Pa with a power of 100 W for 6 min. During the treatment, only the surface printed with MEM was exposed to the plasma. The other side was attached with a glass slice, that is, free from the plasma treatment. After the plasma treatment, the MEM residuum was removed by immersing the PDMS film in the acetic acid (≥99% Sigma-Aldrich) for 5 min and then rinsed by deionized water. After releasing the PDMS, microgrooves were self-formed on the treated surface due to the strain difference between the SiO_x layer and the PDMS beneath. The stretching ratio of the length was 1.6 for all microgrooves generation in this work.

Characterizations: The static water contact angles were measured by a contact angle measuring system (OCA 50, DataPhysics Instruments) at 25 °C under ambient conditions. The surface morphology was measured by AFM (NanoWizard, Bruker Nano), and the surface RMS roughness was analyzed with Gwyddion. Optical images were obtained by a light microscope (Axioplan 2 imaging, Carl Zeiss) equipped with a CCD camera (AxioCam ICc3, Carl Zeiss). The deposited PVA thin layer thickness was measured by a 3D optical profilometer (ContourGT-X, Bruker). SEM images were obtained by SUPRA 55 (Carl Zeiss) at 3 kV. The total and diffusive transmittance spectra were measured with a spectrophotometer (Lambda 1050 UV/vis/NIR, PerkinElmer) under normal incidence and unpolarized light.

Supporting Information

Supporting Information is available from the Wiley Online Library or from the author.

Acknowledgements

The authors wish to acknowledge the Deutsche Forschungsgemeinschaft (DFG, German Research Foundation) under Germany's Excellence Strategy via the Excellence Cluster 3D Matter Made to Order (EXC-2082/1-390761711), and the program DFG-SPP 1839 "Tailored disorder-PROPOLIS" for financial support. J.C. gratefully acknowledges financial support through the Chinese Scholarship Council (201906150139).

Open access funding enabled and organized by Projekt DEAL.

Conflict of Interest

The authors declare no conflict of interest.

Data Availability Statement

The data that support the findings of this study are available from the corresponding author upon reasonable request.

Keywords

inkjet printing, light scattering, micro-etching-mask, smart window display, surface modification

Received: September 2, 2021
Published online:

[1] M. Kriss, *Handbook of Digital Imaging*, Wiley, Chichester **2015**.
[2] M. Fernández, E. Casanova, I. Alonso, *Sustainability* **2015**, *7*, 10854.
[3] B. Comiskey, J. D. Albert, H. Yoshizawa, J. Jacobson, *Nature* **1998**, *394*, 253.
[4] Y. Ke, J. Chen, G. Lin, S. Wang, Y. Zhou, J. Yin, P. S. Lee, Y. Long, *Adv. Energy Mater.* **2019**, *9*, 1902066.
[5] H.-K. Kwon, K.-T. Lee, K. Hur, S. H. Moon, M. M. Quasim, T. D. Wilkinson, J.-Y. Han, H. Ko, I.-K. Han, B. Park, B. K. Min, B.-K. Ju, S. M. Morris, R. H. Friend, D.-H. Ko, *Adv. Energy Mater.* **2015**, *5*, 1401347.
[6] N. DeForest, A. Shehabi, J. O'Donnell, G. Garcia, J. Greenblatt, E. S. Lee, S. Selkowitz, D. J. Milliron, *Build. Environ.* **2015**, *89*, 107.

[7] J. Wang, L. Zhang, Le Yu, Z. Jiao, H. Xie, X. W. D. Lou, X. W. Sun, *Nat. Commun.* **2014**, *5*, 4921.
[8] Y. Chen, L. Fan, Q. Fang, W. Xu, S. Chen, G. Zan, H. Ren, L. Song, C. Zou, *Nano Energy* **2017**, *31*, 144.
[9] H. Khandelwal, R. C. G. M. Loonen, J. L. M. Hensen, M. G. Debije, A. P. H. J. Schenning, *Sci. Rep.* **2015**, *5*, 11773.
[10] D. Ge, E. Lee, L. Yang, Y. Cho, M. Li, D. S. Gianola, S. Yang, *Adv. Mater.* **2015**, *27*, 2489.
[11] P. Kim, Y. Hu, J. Alvarenga, M. Kolle, Z. Suo, J. Aizenberg, *Adv. Opt. Mater.* **2013**, *1*, 381.
[12] H.-N. Kim, D. Ge, E. Lee, S. Yang, *Adv. Mater.* **2018**, *30*, e1803847.
[13] S. Béfahy, P. Lipnik, T. Pardoen, C. Nascimento, B. Patris, P. Bertrand, S. Yunus, *Langmuir* **2010**, *26*, 3372.
[14] S. G. Lee, D. Y. Lee, H. S. Lim, D. H. Lee, S. Lee, K. Cho, *Adv. Mater.* **2010**, *22*, 5013.
[15] Z. Li, Y. Zhai, Y. Wang, G. M. Wendland, X. Yin, J. Xiao, *Adv. Opt. Mater.* **2017**, *5*, 1700425.
[16] M. Ouyang, C. Yuan, R. J. Muisener, A. Boulares, J. T. Koberstein, *Chem. Mater.* **2000**, *12*, 1591.
[17] H. Hillborg, J. F. Ankner, U. W. Gedde, G. D. Smith, H. K. Yasuda, K. Wikström, *Polymer* **2000**, *41*, 6851.
[18] O. S. Krüger, E. H. Saenger, S. A. Shapiro, *Geophys. J. Int.* **2005**, *162*, 25.
[19] T. Trantidou, Y. Elani, E. Parsons, O. Ces, *Microsyst. Nanoeng.* **2017**, *3*, 1.
[20] L. Yu, C. M. Li, Q. Zhou, J. H. T. Luong, *Bioconjugate Chem.* **2007**, *18*, 281.
[21] D. Belder, A. Deege, H. Husmann, F. Kohler, M. Ludwig, *Electrophoresis* **2001**, *22*, 3813.
[22] T. He, Q. Liang, K. Zhang, X. Mu, T. Luo, Y. Wang, G. Luo, *Microfluid. Nanofluid.* **2011**, *10*, 1289.
[23] T. Serizawa, S. Hashiguchi, M. Akashi, *Langmuir* **1999**, *15*, 5363.
[24] S. Zeng, R. Li, S. G. Freire, V. M. M. Garbellotto, E. Y. Huang, A. T. Smith, C. Hu, W. R. T. Tait, Z. Bian, G. Zheng, D. Zhang, L. Sun, *Adv. Mater.* **2017**, *29*, 24.
[25] M. Kozlov, M. Quarmyne, W. Chen, T. J. McCarthy, *Macromolecules* **2003**, *36*, 6054.
[26] J. Y. Park, D. Ahn, Y. Y. Choi, C. M. Hwang, S. Takayama, S. H. Lee, S.-H. Lee, *Sens. Actuators, B* **2012**, *173*, 765.
[27] M.-H. Wu, S.-B. Huang, G.-B. Lee, *Lab Chip* **2010**, *10*, 939.
[28] L. Bi, P. Yang, G. W. Kattawar, *Appl. Opt.* **2010**, *49*, 4641.
[29] P. Yang, L. Bi, B. A. Baum, K.-N. Liou, G. W. Kattawar, M. I. Mishchenko, B. Cole, *J. Atmos. Sci.* **2013**, *70*, 330.
[30] H. M. Nussenzveig, *J. Opt. Soc. Am.* **1979**, *69*, 1068.
[31] Y. C. Agrawal, A. Whitmire, O. A. Mikkelsen, H. C. Pottsmith, *J. Geophys. Res.* **2008**, *113*, C4.
[32] L. Bi, P. Yang, *J. Quant. Spectrosc. Radiat. Transfer* **2016**, *178*, 93.
[33] CVRL database, CIE luminous efficiency functions, CIE $V_m(\lambda)$, http://www.cvrl.org (accessed: August 2021).